ADVANCED NANOBIOMED RESEARCH Open Access
www.advnanobiomedres.com

Detection of Estrogen Receptor Status in Breast Cancer Cytology Samples by an Optical Nanosensor

*Pooja V. Gaikwad, Nazifa Rahman, Pratyusha Ghosh, Dianna L. Ng, and Ryan M. Williams**

Breast cancer is a substantial source of morbidity and mortality worldwide. Estrogen receptor (ER), progesterone receptor (PR), and human epidermal growth factor receptor 2 (HER2) are the primary biomarkers which inform breast cancer treatment. Although endocrine therapy for ER+ patients is widely available, there is a need for increased access to low-cost, rapid, and accurate ER testing methods. In this work, we designed a near-infrared optical nanosensor using single-walled carbon nanotubes (SWCNT) as the transducer and an anti-ERα antibody as the recognition element. We evaluated the nanosensor in vitro prior to testing with 26 breast cancer samples which were collected by scraping the cut surface of fresh, surgically resected tumors. Twenty samples were ER+, and six ER−, representing 13 unique patients. We found that the nanosensor can differentiate ER− from ER+ patient biopsies through a shift in its center wavelength upon sample addition. Receiver operating characteristic area under the curve analyses determined that the strongest classifier with an AUC of 0.94 was the (7,5) SWCNT after direct incubation and measurement, and without further processing. We anticipate that further testing and development of this nanosensor may push its utility toward field-deployable, rapid ER subtyping with the potential for additional molecular marker profiling.

1. Introduction

Breast cancer is one of the leading causes of cancer-related deaths in women in low- and middle-income countries (LMICs),[1] which is in part attributable to the high proportion of patients with advanced disease at the time of diagnosis as well as limited pathology capacity.[2–4] Hence, developing novel technologies that increase access to early and timely diagnosis as well as ancillary testing to determine eligibility for lifesaving targeted therapies is crucial for decreasing the overall mortality rate in resource-constrained settings. Although core needle biopsy is more commonly used than fine-needle aspiration biopsy (FNAB) in high-resource settings, this biopsy method is prohibitively expensive and not readily available in many resource-constrained settings. FNAB is a widely used diagnostic method in LMICs because it requires minimal laboratory infrastructure and cost-effectiveness.[5–7] The technique also allows for diagnosis with high sensitivity and specificity for palpable malignant breast masses.[6]

Estrogen receptor (ER), progesterone receptor (PR), and human epidermal growth factor receptor 2 (HER2) status testing is essential for determining the prognosis as well as appropriate treatment in breast carcinomas.[8] In particular, endocrine therapy is widely available in many low-resource settings and has been shown to significantly improve overall survival and progression-free survival in early-stage disease[9,10] as well as tumor reduction in later-stage disease[11–15] for ER+ tumors. The American Society of Clinical Oncology (ASCO) recommends endocrine therapy as the initial course of treatment for hormone receptor-positive metastatic breast cancer.[12] Conventionally, immunohistochemistry (IHC) is used for ER, PR, and HER2 status testing. However, there are numerous barriers to accessing IHC in LMICs, including few hospitals with pathology services, an insufficient number of trained personnel, reagent and equipment shortages, and suboptimal specimen processing using traditional histology methods. A recent survey of laboratories in sub-Saharan Africa found that only approximately half offered IHC services,[16] but even when available, results can take up to several weeks in low-to-middle-income countries.[17–19] Therefore, novel, rapid, and low-cost methods are needed to improve breast cancer biomarker testing and, in turn, access to critical endocrine therapies.

P. V. Gaikwad, N. Rahman, P. Ghosh, R. M. Williams
Department of Biomedical Engineering
The City College of New York
New York, NY 10031, USA
E-mail: rwilliams4@ccny.cuny.edu

P. V. Gaikwad, R. M. Williams
PhD Program in Chemistry
Graduate Center
City University of New York
New York, NY 10016, USA

D. L. Ng
Department of Pathology and Laboratory Medicine
Memorial Sloan Kettering Cancer Center
New York, NY 10065, USA

The ORCID identification number(s) for the author(s) of this article can be found under https://doi.org/10.1002/anbr.202400099.

DOI: 10.1002/anbr.202400099

Single-walled carbon nanotubes exhibit unique characteristics conducive to signal transduction in biological samples. Semiconducting SWCNT are cylindrical fullerenes with near-infrared (NIR) fluorescence emission, which is relatively unabsorbed by biological tissue.[20,21] There are dozens of semiconducting nanotube species that are defined by an integer (*n*,*m*) index that describes the roll-up vector of a hypothetical graphene sheet, each with discrete, narrow absorption and fluorescence emission bands, and very large Stokes shifts.[20] This portends the possibility of highly multiplexed detection via multiple (*n*,*m*) species.[22,23] Previous work has shown the ability to image nanotubes within biological tissue and in live animals.[24,25] Thus, loss of signal from biomolecule interference is not a concern with nanotube-based sensing as they are in the "tissue window" of the electromagnetic spectrum.[21,22,26–28] Additionally, nanotube fluorescence does not decrease over time as with traditional fluorophores, which has allowed for their frequent and long-term imaging.[21,24,29]

Nanotube-based optical sensors have previously been developed for diverse classes of molecules and have been adapted for rapid disease diagnostics with potential use at the bedside. SWCNT fluorescence is dependent on the local environment; thus, it can be modulated by binding of antigen following functionalization.[30–32] These analytes include small molecules, nucleic acids, lipids, and proteins[21,22,27,28,30–33] Thus, SWCNT are ideal transducers of analyte concentrations. Quantitative sensors for biomolecules in live animals have been developed for the majority of these analytes using strategies ranging from direct injection[21,27] to sensor immobilization in hydrogel matrices or semipermeable membranes.[21,22,28] Further, rapid, ex vivo biological sensors using SWCNT have been characterized for multiple disease biomarkers, including lipids, microRNAs, prostate cancer-specific proteins, and ovarian cancer-specific proteins.[22,27,28,33,34] These have demonstrated functionality in patient serum, urine, cell lines, and ascites.

In this work, we aimed to develop a SWCNT-based rapid detection tool to determine ER status in breast cancer cytology samples. We took inspiration from prior studies which used nonfunctionalized SWCNT sensors to evaluate the presence of proteins on the surface of cells in a nonspecific manner.[34] We combined that with our own prior studies that created a molecularly specific SWCNT-based sensing platform, wherein the SWCNT serves as the signal transduction element and a biomarker-specific antibody serves as the recognition element.[28,33,35] Our prior work with this platform has used antibodies specific for the ovarian cancer biomarker human epididymis protein 4 (HE4),[28] the prostate cancer biomarker urokinase plasminogen activator (uPA),[33] and the inflammatory cytokine interleukin 6 (IL-6).[35] Those published works demonstrated the stability and functionality of this sensor platform, with physicochemical validation primarily focused on dynamic and electrophoretic light scattering to verify conjugation. They also demonstrated a very low limit of detection for this platform of 25 pg mL^{-1} IL-6 in human serum, the ability to detect uPA in human serum and plasma samples, and the ability to detect HE4 in human ascites—as well as in live mouse models of ovarian cancer. Combined, those studies also validate the "plug-and-play" utility of this sensing platform, with the ability to use the same conjugation scheme to detect different biomarkers based on the insertion of commercial antibodies of interest. However, despite the demonstrated effectiveness of this platform, it has only been validated for use in detecting soluble proteins—it has not previously been used for detection of a specific biomarker tethered to the plasma membrane of a cell. Therefore, in this work, we explored the most optimal conditions for detection of the ER on the surface of breast cancer cells using this well-established platform. This substantial advance in this platform is necessary to potentially translate a tool for cancer phenotyping in the field or clinic.

2. Results and Discussion

2.1. Nanosensor Synthesis

The ERα nanosensor was constructed using our previously published carbodiimide chemistry methodology and a monoclonal human anti-ERα antibody.[28,33] The sensing strategy (**Figure 1**A) was that the fluorescence emission profile of the sensor changed upon recognition of ERα. We first determined that the sensor construct exhibited bright, stable fluorescence upon excitation with 638 nm laser light across the NIR spectrum with peaks corresponding to individual nanotube species characteristic of a bulk SWCNT solution (Figure 1B). DLS demonstrated that the correlation coefficient of the nanosensor had a slower decay rate than the unconjugated base ssDNA-SWCNT construct due to a larger hydrodynamic radius caused by the antibody (Figure 1C). Additionally, electrophoretic light scattering shows a more neutral ζ-potential for the ERα nanosensor than that for SWCNT-$(TAT)_6$ (Figure 1D). These physicochemical characterizations have previously been used to validate successful antibody functionalization of the nanotube as indicated by relative changes in size and charge of the complex.[28,33,35]

2.2. Assessing Sensor Response In Vitro

We first evaluated the nanosensor response to 250 nM recombinant ERα in PBS. We found that the center wavelength of (7,6) species of the nanosensor was redshifted by 3.5 ± 0.2 nm compared to no-protein controls ($P = 0.004$) (**Figure 2**A). We then evaluated the sensor response to the same recombinant protein in a solution of 10% serum (FBS) to simulate a complex protein-rich environment. The sensor was passivated with BSA as in our prior work to prevent biofouling.[33,35] We again observed a significant response from the (7,6) species of the nanosensor. In this case, a blueshift of 1.0 ± 0.2 nm was observed ($P = 0.01$) (Figure 2B). It is likely that the center wavelength underwent a blueshift in 10% FBS as opposed to the redshift in serum due to the rearrangement of passivating BSA or loose protein corona formation.

2.3. Differentiation of ER+ and ER− Breast Cancer Cell Lines

We then sought to evaluate the optimal conditions for the detection of ERα on the cell surface. We used two cell lines, ERα-negative MDA-MB-231 and ERα-positive HCC1500 cells. The MDA-MB-231 cell line is a commonly used triple-negative breast cancer (TNBC) cell line, established from a patient with metastatic

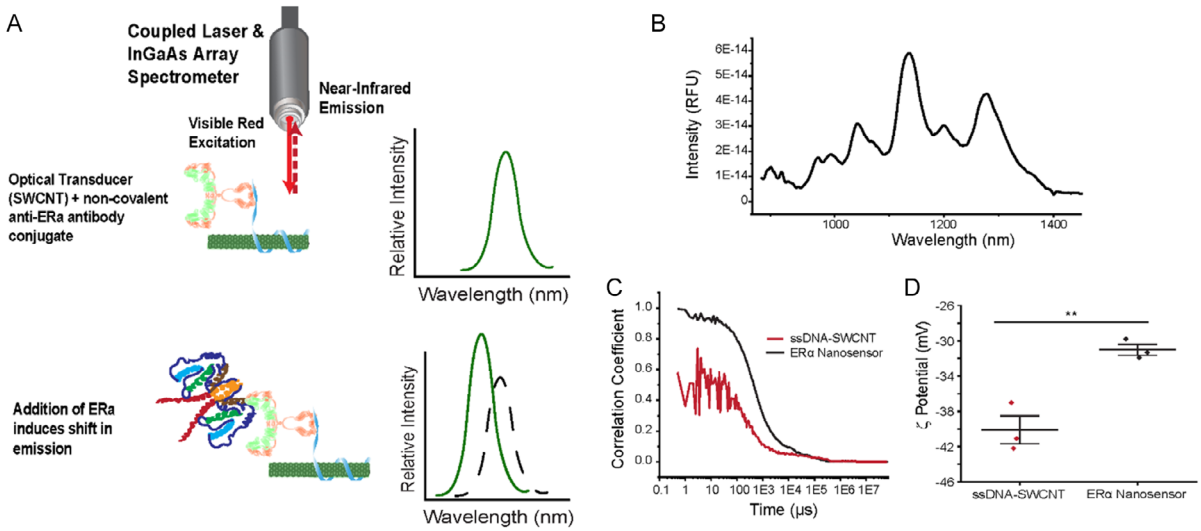

Figure 1. Nanosensor scheme and synthesis. A) Schematic of the ERα antibody-based NIR fluorescent nanosensor detection concept. B) NIR fluorescent spectra of the construct nanosensor in PBS. Success of the antibody conjugation to base construct was assessed by C) comparison of decay in correlation coefficient as a function of time for SWCNT-$(TAT)_6$-NH_2 and ERα antibody (Ab) conjugated to SWCNT-$(TAT)_6$. D) Change in zeta potential for ssDNA-SWCNT compared to the ERα nanosensor. Difference in means = 9.1 mV, $P = 0.006$.

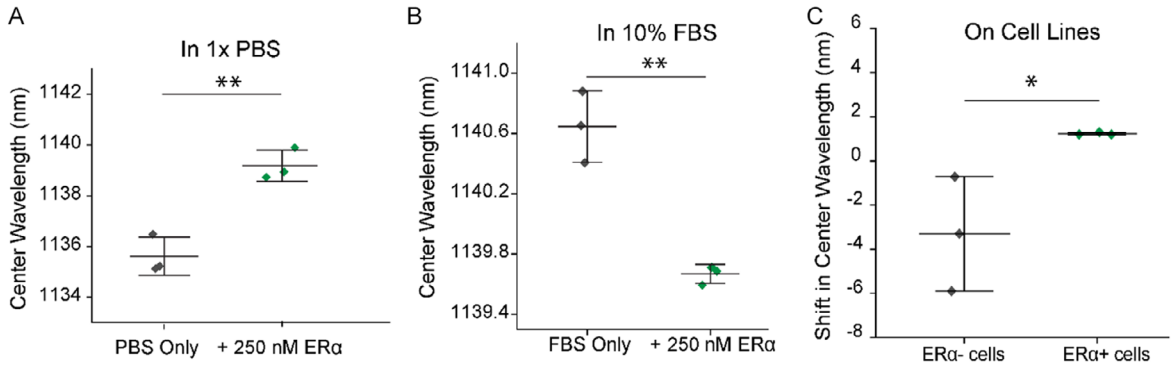

Figure 2. ERα nanosensor response in vitro. A) Response of the (7,6) SWCNT nanosensor to 250 nM recombinant ERα in PBS. Difference in means = 3.5 nm, $P = 0.004$. B) Response of the nanosensor (7,6) SWCNT to 250 nM recombinant ERα in 10% FBS. Difference in means = 1.0 nm, $P = 0.002$. C) Change in the center wavelength of the (7,5) SWCNT for the nanosensor incubated with ER− or ER+ cells. Difference in means = 4.5 nm, $P = 0.04$. $n = 3$ replicates per group; summary statistics are represented by mean (center line) and standard deviation (error bars). Two-tailed *t*-tests were performed.

mammary adenocarcinoma.[36] It lacks expression of ER, PR, and human epidermal growth factor receptor (HER2).[37,38] HCC1500 was established from a patient with ductal carcinoma and has ER and PR expression.[39] Cells were formalin-fixed and suspended in PBS to simulate the environment of fixed patient samples.

Cells collected from this method were counted to obtain $12.8 \pm 5.6\ E^5\ mL^{-},^1$ whereas a control sample obtained by enzymatic digestion (TrypLE) yielded $15.7 \pm 0.9\ E^5\ mL^{-1}$ cells. After 30 min of incubation, we observed that the (7,5) species demonstrated a 3.3 ± 2.6 nm blueshift after incubation with ERα−, whereas ERα+ cells induced a 1.2 ± 0.02 nm redshift ($P = 0.04$) (Figure 2C). These results indicate that there is indeed a differential response of the sensor when incubated with TNBC versus ER+ breast cancer cell lines. That the directionality of the difference was a net redshift of ≈4.5 nm indicates that sensor response was most like that of PBS conditions (Figure 2A) as there was no heterogenous formation of protein corona on the sensor. This overall difference in the (7,5) center wavelength in response to the two cell lines is 4.5 nm, corresponding to a change in photon energy of ≈4.5 meV. Changes of this approximate magnitude, and smaller, have been previously demonstrated to be sufficient for detection in patient serum, ascites, and protein biomarkers in vivo.[28,33] We therefore concluded that further testing on patient samples with the sensor was appropriate.

2.4. Sensor Response to Breast Cancer Cytology Samples

We then sought to determine the optimal conditions for sensor performance with FNAB-mimic patient samples and to evaluate whether the sensor can differentiate patient tumor samples

which are ER− from ER+. The sensor performance was compared directly to immunohistochemistry (IHC)-based determinations of ER status in these patient samples. To do so, we first measured the sensor fluorescence before and after the addition of 10 µL (10% of the total solution) of the patient sample. Each sample was measured in triplicate and the shift in center wavelength at the 90 min timepoint from prior to addition for each was determined as an average of the three measurements. In total, IHC determined that six samples (from three unique patients) were ER− while 20 samples (from ten unique patients) were ER+.

The first condition we evaluated was the direct addition of patient samples to the sensor with no further processing (**Figure 3**A). We observed three separate SWCNT species, the (7,5), (7,6), and (9,4), to determine which were optimal for sample differentiation. We found that for all three, a redshift occurred in response to ER− patient samples of 1.8 ± 1.7, 2.3 ± 1.1, and 1.1 ± 0.7 nm, respectively (Figure 3B–D). In each case, the average of the ER+ exposed sensor underwent a lower-magnitude redshift or a blueshift, with a difference in center wavelength shift of 2.3, 1.6, and 1.2 nm, respectively. Each difference in means was statistically significant ($P = 0.001$, 0.0002, and 0.0001, respectively) (Figure 3B–D).

It is notable that the largest-magnitude shift of the (7,5) SWCNT gives the clearest distinction between populations. At a cutoff of between 0.4 and 0.7 nm wavelength shift, only two of the samples would be misclassified based on overlap between sensor responses (specifically two ER+ samples). From a sensor response point of view, we found it notable that the sensor response more closely resembled the response in 10% FBS, whereas cell line experiments more closely resemble those in PBS. We surmise this is due to the cell line experiments being performed with washed cells in PBS, while patient biopsy samples were scrapings of whole tissue, which included both tumor tissue, extracellular matrix, and other components—more closely resembling the complex protein-rich environment of FBS.

To further evaluate which individual SWCNT response was the most optimal, we evaluated the area under the curve of the receiver operator characteristic. We found that the AUC for the (7,5), (7,6), and (9,4) responses were 0.94, 0.85, and 0.91, respectively ($P = 0.0029$, 0.017, and 0.0020, respectively) (Figure 3E). We therefore concluded that each of the three evaluated (n,m) species was able to differentiate between ER− and ER+ tumor tissue with substantial accuracy. However, the (7,5) SWCNT demonstrated both the largest difference in means of center wavelength shifts as well as the greater AUC. Specifically, the (7,5) SWCNT demonstrated a 94% accuracy in the differentiation of ER− and ER+ tumor tissue, with only two samples misclassified at a cutoff of 0.4–0.7 nm redshift from baseline.

At the same time, we sought to determine whether samples processed to remove unbound sensor were comparable or better

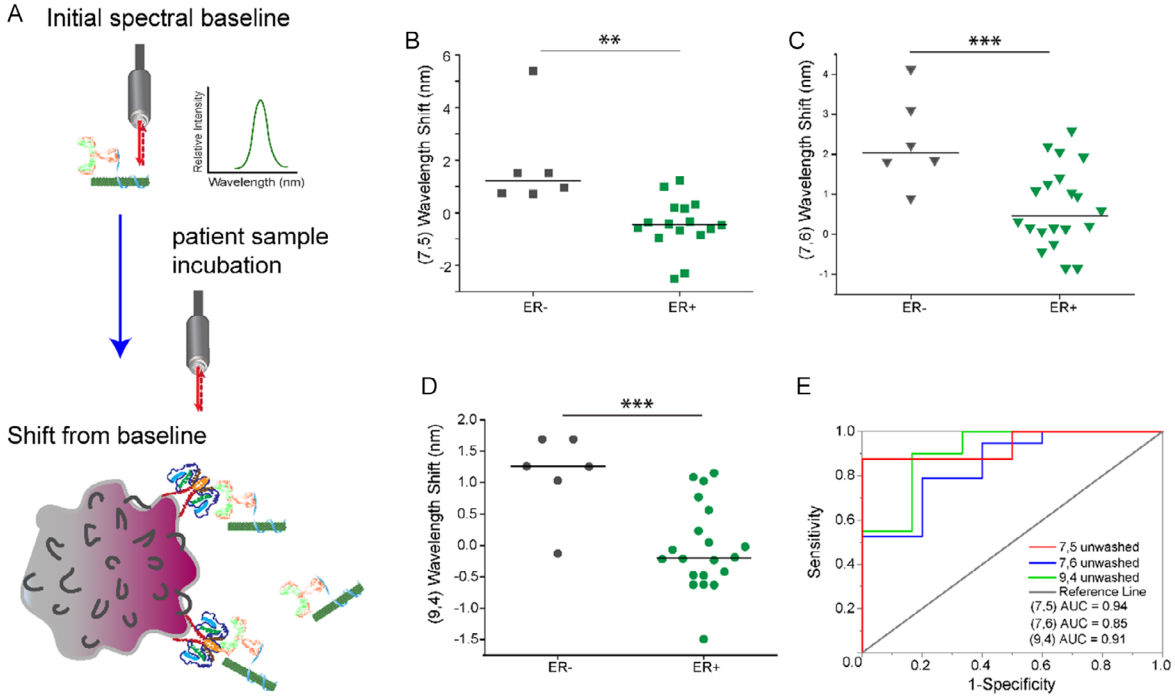

Figure 3. Nanosensor response to breast cancer cytology samples. A) Schematic of direct nanosensor response measurement to ER+ breast cancer patient cells. B) Change in the center wavelength of the (7,5) SWCNT nanosensor after incubation with ER− or ER+ breast cancer scrapings. Difference in means = 2.3 nm, $P = 0.0011$. C) Change in the center wavelength of the nanosensor (7,6) SWCNT after incubation with ER− or ER+ breast cancer scrapings. Difference in means = 1.6 nm, $P = 0.0002$. D) Change in the center wavelength of the nanosensor (9,4) SWCNT after incubation with ER− or ER+ patient samples. Difference in means = 1.2 nm, $P = 0.0001$. E) Receiver operating characteristic evaluation of the ability of each (n,m) species to differentiate ER− from ER+ scrapings. AUC is area under the curve. $P(7,5) = 0.0020$, (7,6) = 0.017, (9,4) = 0.0029. For (B–D), $n = 6$ samples in ER− group and $n = 16$ and 20 samples in ER+ group (points discarded if signal was too dim for pseudo-Voigt fitting of $R^2 > 0.95$), summary statistics are represented by mean (center line) and standard deviation (error bars), and two-tailed t-tests were performed.

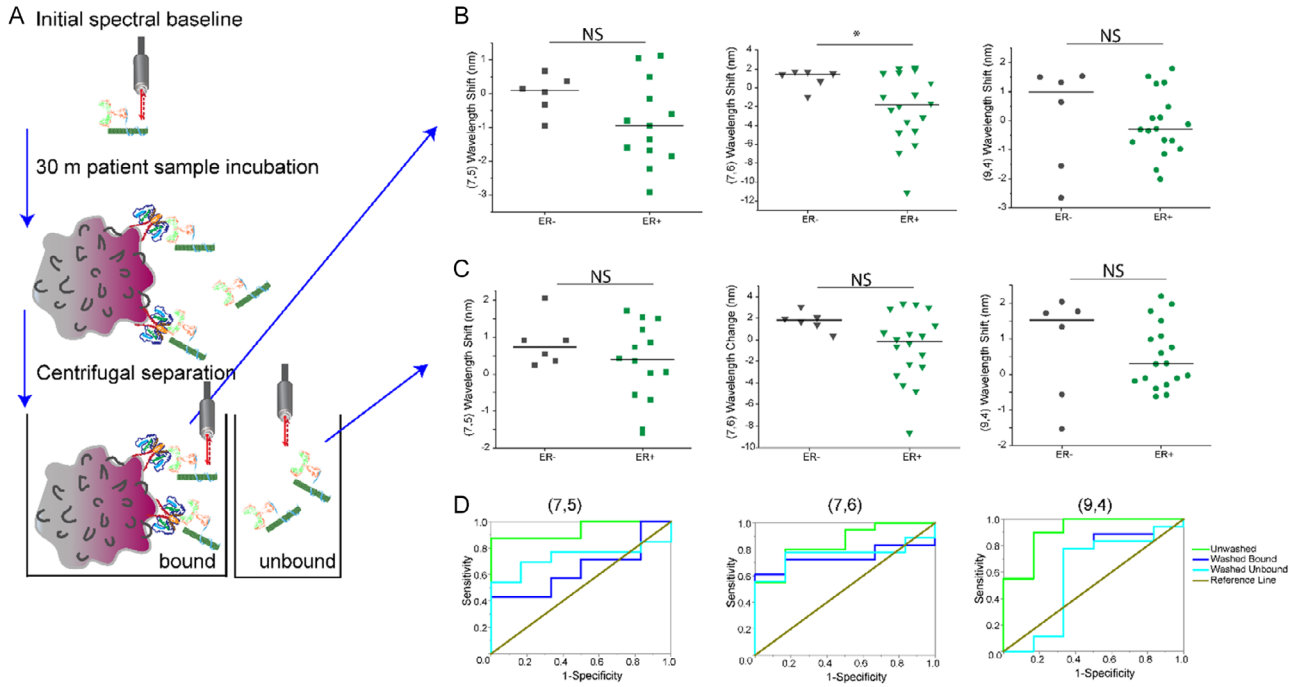

Figure 4. Comparison of fractionation method versus direct measurement. A) Schematic representing the fractionation method to measure the change in center wavelength for bound versus unbound nanosensors. B) Change in the center wavelength of each SWCNT nanosensor species for the "Washed Bound" fraction. Only the (7,6) SWCNT exhibited a significant change. Difference in means = 3.1 nm, $P = 0.025$. C) Change in the center wavelength of the nanosensor each species of the "Washed Unbound" fraction. No differences were statistically significant. D) ROC comparison of the three measurements (from Figure 3 and 4) and the ability of each (n,m) species to differentiate ER− from ER+ cells. Only the unwashed method was statistically significant (please refer to Figure 3 for AUC and P values for each). For (B,C), $n = 6$ samples in the ER− group and 13, 16, and 17 samples in the ER+ group (points discarded if the signal was too dim for suitable pseudo-Voigt fitting of $R^2 > 0.8$); summary statistics are represented by mean (center line) and standard deviation (error bars), and two-tailed t-tests were performed.

than the direct-incubation method above. In this experimental design, sensor that was bound to the cells was separated from sensor remaining in solution via centrifugation after a 30 min incubation (**Figure 4**A). First, we found that, due to the fractionation protocol, 6–7 of the samples were not sufficiently bright enough for data analysis. Of those that were bright enough in the "washed bound" fraction containing sensor bound to cells, we found again that ER− cells induced a redshift, while ER+ cells induced a blueshift. However, only the difference in means of the (7,6) SWCNT, at 3.1 nm was statistically significant ($P = 0.025$) (Figure 4B). Each of the other species demonstrated a trend in the data showing the same blueshifted phenomenon for ER+ cells; however, several outlier samples existed. This was likely due to low-intensity spectra from having removed much of the sensor.

We then evaluated the sensor change for the "unbound wash" fraction or the sensor which was not bound to cells. We hypothesized that no difference would be present in these samples as the ER is found on the cell surface, though it is acknowledged that aspiration could sheer some cells, releasing membrane proteins that are not bound to cells. Despite this possibility, we found the expected result of no significant difference in the sensor in solution after incubation with ER− or ER + FNAB mimics (Figure 4C).

Finally, we performed an AUC analysis of ROC curves to compare the ability of the sensor to discern ER− from ER+ tumor samples in each of the three preparation conditions: unwashed, washed bound, and washed unbound. For the (7,5) SWCNT, we found that only the "unwashed" preparation could reliably differentiate the samples (AUC and P values reported above), with neither of the other preparations being significant ($P < 0.05$) (Figure 4D). Likewise, for the (7,6) and (9,4) species, again only the "unwashed" sample was statistically significant. We therefore concluded that the minimal processing associated with direct measurement and no fractionation was optimal, likely due to improved signal relative to noise.

3. Conclusions

In this work, we found that an engineered optical nanosensor for ER can successfully differentiate ER− from ER+ breast cancer samples with substantial accuracy. We established an optimized methodology for cytologic samples with our nanosensor, which operated within 90 min. We believe this work has substantial potential for rapid differentiation of ER status in the field or in low-resource settings, which would likely require other more traditional diagnostic methods to determine the actual presence of breast cancer itself.

Despite this potential, we also recognize that additional studies regarding the stability and sensitivity of the SWCNT-based sensor are necessary. And, while SWCNT-based sensor platforms are a

burgeoning field of research, substantially more studies have been performed to improve the sensitivity and stability of other sensor platforms. Excellent examples of such high-sensitivity patient sample diagnostic sensor include FET-based electrochemical, evanescent wave-based sensors, and Raman-based sensors.[40–43] Further, as SWCNT fluorescence is in the NIR, we also recognize that codevelopment of field-deployable, low-cost spectroscopic methods is necessary for the preclinical development of this tool for LMIC, though the other examples above also require codevelopment of complementary tools. We also anticipate multiplexation of this sensor device to evaluate PR and HER2 status at the same time. Finally, we plan to perform larger-scale screens in a broader patient population to approach quantitative stratification of the relative abundance of ER+ cells. We are hopeful that this work will reduce the cost and speed necessary for proper diagnosis, allowing proper treatment regimens to be tailored to each patient.

4. Experimental Section

Preparation of SWCNT-ssDNA: HiPCO-prepared SWCNT were suspended in a solution with $(TAT)_6$-NH_2 ssDNA as described in our prior work.[35] The concentration of this base construct was obtained also as before.[28,33,35,44]

ERα Nanosensor Synthesis: Conjugation of the primary amine-functionalized ssDNA-SWCNT construct was performed with a monoclonal ERα antibody that had been demonstrated for recognition of both solubilized and surface-bound ERα (Catalog # 14-9740-82, Invitrogen, Massachusetts, USA) using carbodiimide conjugation chemistry identically to previous studies.[28,33,35]

Physicochemical Characterization of the ERα Nanosensor: The antibody-functionalized nanosensor construct was characterized via dynamic light scattering and electrophoretic light scattering identically to our prior studies.[28,33,35] The use of such technology to evaluate size, and relative size, of carbon nanotubes has been performed by several other groups.[45–48]

Characterization of Sensor Response to ERα in Solution: To evaluate the basic functionality of the ERα nanosensor complex in buffer, we first measured the fluorescence response of 0.5 mg L^{-1} nanosensor to 250 nM human ERα (Catalog number NBP2-34478PEP, Novus Biologicals; Colorado, USA) in 1× PBS using a NIR fluorescent cuvette-based spectrometer (NS MiniTracer; Applied NanoFluorescence, Texas, USA), which has been previously been described in our and other works.[49–53] In triplicate, samples containing 0.5 mg L^{-1} nanosensor were spiked with 250 nM ERα. Data was acquired for time points 2, 15, 30, 60, 120, and 180 min after the addition of ERα antigen. The exposure time used was 3000 ms, with 3 spectra taken and averaged. The instrument excitation wavelength was 638 nm (100 mW laser) and emission was collected from 900 to 1600 nm via InGaAs array.

We then measured sensor response in 10% fetal bovine serum (heat-inactivated FBS; Corning, New York, USA). Prior to the addition of ER, the nanosensor was passivated with 50× mass excess of bovine serum albumin (BSA; Fisher Scientific) than the nanosensor for 30 min at 4 °C as in our prior serum studies.[28,33] Data was acquired as described above. All experiments were performed in triplicate.

Custom MATLAB code was used to analyze and fit individual nanotube (*n*,*m*) species peaks to a pseudo-Voigt model (code available upon request). Separate SWCNT species were defined by a (*n*,*m*) index which describes the roll-up vector of a single sheet of sp^2 hybridized carbon atoms, as in a graphene sheet.[20,54] These denote separate SWCNT species, each with a different helical angle of the carbon lattice, different excitation and emission maxima, and therefore different electron band structures. While separate (*n*,*m*) species may be obtained and used in multiplexed sensing,[23] in this work, we used mixed preparations and reported the results from prominently abundant species. Therefore, we analyzed fluorescence emission from the following nanotube species excited by the 638 nm laser source: (7,5), (7,6), and (9,5). Fits were ensured to have goodness of fit values (R^2) greater than 0.98 prior to analyses. Center wavelengths were obtained from each fit, as well as maximum intensity values.

Characterization of Sensor Response in Immortalized Cell Culture Models: MDA-MB-231 cells (American Type Culture Collection/ATCC; Virginia, USA) known to lack ERα[37] were cultured in filter-purified 1× DMEM media (Corning) supplemented with 10% FBS and 1× pen/strep (Sigma). HCC1500 (ATCC CRL-2329) cells known to express ERα[55] were cultured in filtered RPMI-1640 media (Corning) with 10% FBS and 1× primocin (InvivoGen; California, USA).

Cells were passaged in T75 culture flasks after reaching 80%–90% confluency via 1× TrypLE Express (Fisher) with regular media changes as necessary, with propagation at 37 °C with 5% CO_2 and humidity. Cell counts and viability assays were performed via Trypan blue exclusion and a Countess automated cell counter (Invitrogen).

To evaluate the nanosensor response to each cell line, cells were seeded into a six-well plate with 30 000 cells per well prior to incubation for 3 days. Cells were washed with PBS and fixed with 1 mL 10% formalin (Fisher) for 45 min at 37 °C. After incubation, cells were scraped and recovered by centrifugation. Cells were resuspended in 500 µL of PBS and diluted with ERα nanosensor solution at a concentration of 0.5 mg L^{-1} SWCNT. The final cell count was 0.2×10^6 cells mL^{-1} and cells were incubated for 15 min at 37 °C. All samples were centrifuged at 4000 g for 10 min, and cell pellets were resuspended in 400 µL PBS.

NIR fluorescence was collected for resuspended triplicates via the MiniTracer cuvette-based spectrometer. Spectral collection parameters were as above for solution-based measurements.

Breast Cancer Patient Sample Collection: Twenty-six total breast cancer samples were collected under Institutional Review Board (IRB) approval at Memorial Sloan Kettering Cancer Center (protocol 20-312). Samples for nanosensor testing were collected from fresh, surgically resected breast tumors by gently scraping the cut surface of the primary tumor with a surgical blade to simulate an FNAB sample (ex vivo FNAB-mimic sample). If the tumor had a malignant diagnosis on prior clinical biopsy, a matched benign sample was also collected by scraping a grossly normal area of the surgical resection.

The scrapings were then rinsed and suspended in 500 µL PBS or tap water. A direct smear slide was also made using tumor scraping. The slide was stained with Quik-Dip (Mercedes Scientific, Lakewood Ranch, FL) and reviewed by a pathologist (Ng) to confirm the cell type and approximate specimen cellularity. The cytologic samples were stored at −80 °C and shared with The City College of New York under Materials Transfer Agreement (MTA). The surgical resections then underwent routine clinical diagnosis, including pathologic review and IHC using validated protocols in a Clinical Laboratory Improvement Amendments (CLIA)-approved laboratory. Interpretation of ER IHC results was done following the American Society of Clinical Oncology (ASCO)/College of American Pathologists (CAP) guidelines.[56] In total, six breast cancer tumor samples that were negative for ERα expression by IHC were used, with two samples derived from three unique patients. For this study, 20 tumor samples were used that demonstrated 95% ($n = 4$) or 99% ($n = 16$) ERα positivity by IHC, with two samples derived from ten unique patients.

Optimization and Characterization of Sensor Response to Patient Samples: The ERα nanosensor was passivated with a 50× mass excess of BSA for 30 min on ice. The sensor was diluted to 0.5 mg L^{-1} at a volume of 90 uL in a 96-well plate (Corning). NIR spectra were acquired using a custom-built high-throughput plate reader spectrophotometer (ClaIR, Photon Etc.; Quebec, Canada), as described in our prior studies.[49–51] Laser excitation of 655 and 730 nm were used sequentially at a power of 1750 mW and an integration time of 750 ms. Spectra were acquired prior to the addition of patient samples, and then, 10 µL of each breast cancer patient sample was added in triplicate. Spectra were collected at 2, 30, 60, 90, 120, 150, and 180 min postsample addition. Custom MATLAB code was used to perform background subtraction and fit individual nanotube (*n*,*m*) species. The analyzed fluorescence emission peaks corresponded to the (7,5), (7,6), and (9,5) species for excitation with the 655 nm laser source and (10,2), (9,4), (8,6), and (8,7) for excitation with the 730 nm laser source.

Fits with $R^2 > 0.95$ were considered for further analysis. Data were reported as an average shift from the presample spectra. As these samples were directly mixed and measured with no further processing, they were designated "unwashed" to differentiate them from further processing below.

We further evaluated whether additional processing was necessary for optimal ERα detection in patient samples. Again, BSA-passivated nanosensor was diluted to 0.5 mg L^{-1} in PBS and spectra were obtained in a 96-well plate (ClaIR plate reader). Then, 10 µL of each sample was added in triplicate and incubated for 30 min. The samples were transferred to microcentrifuge tubes and centrifuged at 4000 g for 10 min. The supernatant was collected, consisting of SWCNT not bound to cells—which we designated as the "washed unbound" fraction. The cell pellet was resuspended in 100 µL PBS, which we designed as the "washed bound" fraction. Each fraction was returned to a 96-well plate and measured with the same parameters as above. Because of the fractionation, samples were dimmer and more difficult to fit. Therefore, only the brightest peaks pertaining to the (7,5), (7,6), and (9,4) species exhibited $R^2 > 0.8$ after fitting to the pseudo-Voigt curve and were used for analysis—fits that did not reach that mark were omitted (seven omissions for "washed bound" fraction and six for the "washed unbound" fraction).

Statistical Analysis and Data Processing Preprocessing of Data: Custom MATLAB code was used to fit individual nanotube (*n*,*m*) species peaks to a pseudo-Voigt model (code available upon request). We analyzed fluorescence emission from the following prominent nanotube species excited by the 638 nm laser source with the cuvette reader: (7,5), (7,6), and (9,5). The analyzed fluorescence emission peaks corresponded to the (7,5), (7,6), and (9,5) species for excitation with the 655 nm laser source and (10,2), (9,4), (8,6), and (8,7) for excitation with the 730 nm laser source for the plate reader. Fits were ensured to have goodness of fit values (R^2) greater than 0.98 prior to analyses in solution and 0.95 in unprocessed patient samples and 0.8 in processed patient samples due to sensor dilution and fractionation. Center wavelengths were obtained from each fit, as well as maximum intensity values.

Data Presentation: Data were presented as shifts in center wavelength from prior to incubation with samples. Graphs show individual points per biological replicate/patient sample with mean ± standard deviation represented by the center bar and error bars in graphics. Summary statistics were reported to one significant digit past the decimal, which was within the precision of instrumentation used.[35,49,57]

Sample Size: In vitro studies in PBS, serum, or cell lines were $n = 3$. Ex vivo studies used 6 ER− patient samples and 20 ER+ patient samples; however, data included in analyses were 6 for ER− and 13–20 for various (*n*,*m*) species and sample processing/fractionation steps, as determined by goodness-of-fit and noted in each graph.

Statistical Methods: Comparison of two groups was performed via a two-tailed *T*-test. *P*-values were assigned $^{***} = P < 0.001$, $^{**} = P < 0.01$, and $^{*} = P < 0.05$. Receiver operating characteristic (ROC) curves were plotted in OriginPro to determine the sensing ability of each (*n*,*m*) species evaluated and each preparation method to differentiate ER− from ER+ tumor samples. Area under the curve (AUC) was calculated as the primary output of this analysis with asymptotic probability used to determine whether the distinction was significant.

Statistical Software: All statistical analyses were performed in OriginPro 2021 (OriginLab Corporation; Massachusetts, USA).

Acknowledgements

The authors wish to acknowledge all members of the Williams Lab for discussion and feedback. This work was supported by the CCNY-MSKCC Partnership for Cancer Research, Education, and Community Outreach (U54CA132378/U54CA137788) (RMW and DLN), The City College of New York Grove School of Engineering (RMW), the National Institutes of Health (K08CA263299) (DLN), and Cancer Center Support Grant (P30CA008748) (DLN). It was also supported by a Dissertation Year Fellowship to P. Gaikwad from the CUNY Graduate Center.

Conflict of Interest

The authors declare no conflict of interest.

Author Contributions

Pooja V. Gaikwad: Formal analysis (lead); Investigation (lead); Methodology (lead); Writing—original draft (lead); Writing—review & editing (lead). **Nazifa Rahman**: Formal analysis (supporting); Investigation (supporting); Methodology (supporting); Writing—review & editing (supporting). **Pratyusha Ghosh**: Investigation (supporting); Methodology (supporting). **Dianna L. Ng**: Data curation (supporting); Formal analysis (supporting); Funding acquisition (lead); Investigation (supporting); Methodology (supporting); Resources (supporting); Writing—original draft (lead); Writing—review & editing (lead). **Ryan M. Williams**: Conceptualization (lead); Data curation (supporting); Formal analysis (lead); Funding acquisition (lead); Methodology (supporting); Project administration (lead); Resources (lead); Supervision (lead); Visualization (supporting); Writing—original draft (lead); Writing—review & editing (lead).

Data Availability Statement

The data that support the findings of this study are available from the corresponding author upon reasonable request.

Keywords

breast cancer, carbon nanotubes, cytology, fluorescence, sensor devices

Received: July 1, 2024
Revised: November 8, 2024
Published online:

[1] H. Sung, J. Ferlay, R. L. Siegel, M. Laversanne, I. Soerjomataram, A. Jemal, F. Bray, *CA Cancer J. Clin.* **2021**, *71*, 209.
[2] Z. He, Z. Chen, M. Tan, S. Elingarami, Y. Liu, T. Li, Y. Deng, N. He, S. Li, J. Fu, W. Li, *Cell Prolif.* **2020**, *53*, e12822.
[3] S. Łukasiewicz, M. Czeczelewski, A. Forma, J. Baj, R. Sitarz, A. Stanisławek, *Cancers* **2021**, *13*, 4287.
[4] Y. M. Martei, L. E. Pace, J. E. Brock, L. N. Shulman, *Clin. Lab. Med.* **2018**, *38*, 161.
[5] Y.-H. Yu, W. Wei, J.-L. Liu, *BMC Cancer* **2012**, *12*, 41.
[6] A. Nerurkar, P. Osin, *Breast Cancer Res.* **2003**, *5*, 305.
[7] J. Thomas, *Int. Health* **2011**, *3*, 3.
[8] K. Geethamala, V. S. Murthy, B. R. Vani, M. S. Rao, M. U. Thejaswini, K. P. Padmaja, *J. Lab. Physicians* **2017**, *9*, 5.
[9] Early Breast Cancer Trialists' Collaborative Group, *Lancet* **2005**, *365*, 1687.
[10] Early Breast Cancer Trialists' Collaborative Group, *Lancet* **2011**, *378*, 771.
[11] W. Eiermann, S. Paepke, J. Appfelstaedt, A. Llombart-Cussac, J. Eremin, J. Vinholes, L. Mauriac, M. Ellis, M. Lassus, H. Chaudri-Ross, *Ann. Oncol.* **2001**, *12*, 1527.
[12] H. S. Rugo, R. B. Rumble, E. Macrae, D. L. Barton, H. K. Connolly, M. N. Dickler, L. Fallowfield, B. Fowble, J. N. Ingle, M. Jahanzeb, *J. Clin. Oncol.* **2016**, *34*, 3069.
[13] I. E. Smith, M. Dowsett, S. R. Ebbs, J. M. Dixon, A. Skene, J.-U. Blohmer, S. E. Ashley, S. Francis, I. Boeddinghaus, G. Walsh, *J. Clin. Oncol.* **2005**, *23*, 5108.

[14] B. Mlineritsch, C. Tausch, C. Singer, G. Luschin-Ebengreuth, R. Jakesz, F. Ploner, M. Stierer, E. Melbinger, C. Menzel, A. Urbania, *Breast Cancer Res. Treat.* **2008**, *112*, 203.
[15] G. Allevi, C. Strina, D. Andreis, V. Zanoni, L. Bazzola, S. Bonardi, C. Foroni, M. Milani, M. R. Cappelletti, F. Gussago, *Br. J. Cancer* **2013**, *108*, 1587.
[16] H.-V. Ziegenhorn, K. G. Frie, I.-O. Ekanem, G. Ebughe, B. Kamate, C. Traore, C. Dzamalala, O. Ogunbiyi, F. Igbinoba, B. Liu, *BMC Health Serv. Res.* **2020**, *20*, 912.
[17] M. Songiso, L. F. Pinder, J. Munalula, A. Cabanes, S. Rayne, S. Kapambwe, A. Shibemba, G. P. Parham, *JCO Global Oncol.* **2020**, *6*, 859.
[18] R. A. Errea, P. J. Garcia, L. E. Pace, J. T. Galea, M. F. Franke, *BMJ Open* **2022**, *12*, e050457.
[19] R. J. Bleicher, *Ann. Surg. Oncol.* **2018**, *25*, 2829.
[20] S. M. Bachilo, M. S. Strano, C. Kittrell, R. H. Hauge, R. E. Smalley, R. B. Weisman, *Science* **2002**, *298*, 2361.
[21] N. M. Iverson, P. W. Barone, M. Shandell, L. J. Trudel, S. Sen, F. Sen, V. Ivanov, E. Atolia, E. Farias, T. P. McNicholas, *Nat. Nanotechnol.* **2013**, *8*, 873.
[22] J. D. Harvey, P. V. Jena, H. A. Baker, G. H. Zerze, R. M. Williams, T. V. Galassi, D. Roxbury, J. Mittal, D. A. Heller, *Nat. Biomed. Eng.* **2017**, *1*, 0041.
[23] R. Nißler, J. Ackermann, C. Ma, S. Kruss, *Anal. Chem.* **2022**, *94*, 9941.
[24] G. Hong, S. Diao, J. Chang, A. L. Antaris, C. Chen, B. Zhang, S. Zhao, D. N. Atochin, P. L. Huang, K. I. Andreasson, *Nat. Photonics* **2014**, *8*, 723.
[25] D. Ghosh, A. F. Bagley, Y. J. Na, M. J. Birrer, S. N. Bhatia, A. M. Belcher, *Proc. Natl. Acad. Sci.* **2014**, *111*, 13948.
[26] J. D. Harvey, R. M. Williams, K. M. Tully, H. A. Baker, Y. Shamay, D. A. Heller, *Nano Lett.* **2019**, *19*, 4343.
[27] T. V. Galassi, P. V. Jena, J. Shah, G. Ao, E. Molitor, Y. Bram, A. Frankel, J. Park, J. Jessurun, D. S. Ory, *Sci. Transl. Med.* **2018**, *10*, eaar2680.
[28] R. M. Williams, C. Lee, T. V. Galassi, J. D. Harvey, R. Leicher, M. Sirenko, M. A. Dorso, J. Shah, N. Olvera, F. Dao, D. A. Levine, D. A. Heller, *Sci. Adv.* **2018**, *4*, eaaq1090.
[29] J. T. Robinson, G. S. Hong, Y. Y. Liang, B. Zhang, O. K. Yaghi, H. J. Dai, *J. Am. Chem. Soc.* **2012**, *134*, 10664.
[30] D. A. Heller, E. S. Jeng, T.-K. Yeung, B. M. Martinez, A. E. Moll, J. B. Gastala, M. S. Strano, *Science* **2006**, *311*, 508.
[31] D. A. Heller, H. Jin, B. M. Martinez, D. Patel, B. M. Miller, T.-K. Yeung, P. V. Jena, C. Höbartner, T. Ha, S. K. Silverman, *Nat. Nanotechnol.* **2008**, *4*, 114.
[32] D. A. Heller, G. W. Pratt, J. Zhang, N. Nair, A. J. Hansborough, A. A. Boghossian, N. F. Reuel, P. W. Barone, M. S. Strano, *Proc. Natl. Acad. Sci.* **2011**, *108*, 8544.
[33] R. M. Williams, C. Lee, D. A. Heller, *ACS Sens.* **2018**, *3*, 1838.
[34] D. Roxbury, P. V. Jena, Y. Shamay, C. P. Horoszko, D. A. Heller, *ACS Nano* **2016**, *10*, 499.
[35] P. Gaikwad, N. Rahman, R. Parikh, J. Crespo, Z. Cohen, R. M. Williams, *ACS Appl. Mater. Interfaces* **2024**, *16*, 27102.
[36] R. Cailleau, M. Olivé, Q. V. Cruciger, *In Vitro* **1978**, *14*, 911.
[37] K. J. Chavez, S. V. Garimella, S. Lipkowitz, *Breast Dis.* **2010**, *32*, 35.
[38] H. Liu, C. Zang, M. H. Fenner, K. Possinger, E. Elstner, *Breast Cancer Res. Treat.* **2003**, *79*, 63.
[39] J. L. Tapia, J. C. McDonough, E. L. Cauble, C. G. Gonzalez, D. K. Teteh, L. S. Treviño, *J. Endocr. Soc.* **2023**, *7*, bvad080.
[40] J. Ma, M. Du, C. Wang, X. Xie, H. Wang, T. Li, S. Chen, L. Zhang, S. Mao, X. Zhou, *ACS Sens.* **2021**, *6*, 3367.
[41] B. Wang, L. Liu, H. Zhang, Z. Wang, K. Chen, B. Wu, L. Hu, X. Zhou, L. Liu, *Anal. Chim. Acta* **2024**, *1301*, 342475.
[42] Y. Chen, Y. Zhang, F. Pan, J. Liu, K. Wang, C. Zhang, S. Cheng, L. Lu, W. Zhang, Z. Zhang, *ACS Nano* **2016**, *10*, 8169.
[43] Y. Ma, J. Chi, Z. Zheng, A. Attygalle, I. Y. Kim, H. Du, *J. Biophotonics* **2021**, *14*, e202000275.
[44] J. Zhang, S. Kruss, A. J. Hilmer, S. Shimizu, Z. Schmois, F. De La Cruz, P. W. Barone, N. F. Reuel, D. A. Heller, M. S. Strano, *Adv. Healthcare Mater.* **2014**, *3*, 412.
[45] S. Fujii, S.-I. Honda, Y. Oka, Y. Kuwahara, T. Saito, *Materials* **2023**, *16*, 466.
[46] A. Krasulina, Y. Myasnikova, V. Saik, M. Predtechensky, S. N. Smirnov, *ACS Omega* **2023**, *8*, 39233.
[47] D. Chowdhury, Z. Cui, *Carbon* **2011**, *49*, 862.
[48] B. Krause, M. Mende, P. Pötschke, G. Petzold, *Carbon* **2010**, *48*, 2746.
[49] A. K. Ryan, S. Rahman, R. M. Williams, *ACS Sens.* **2024**, *9*, 3697.
[50] P. Gaikwad, N. Rahman, R. Parikh, J. Crespo, Z. Cohen, R. M. Williams, *ACS Appl. Mater. Interfaces* **2024**, *16*, 27102.
[51] Z. Cohen, D. J. Alpert, A. C. Weisel, A. Ryan, A. Roach, S. Rahman, P. V. Gaikwad, S. B. Nicoll, R. M. Williams, *Adv. Opt. Mater.* **2024**, *12*, 2303324.
[52] P. Cherukuri, C. J. Gannon, T. K. Leeuw, H. K. Schmidt, R. E. Smalley, S. A. Curley, R. B. Weisman, *Proc. Natl. Acad. Sci.* **2006**, *103*, 18882.
[53] R. Wang, P. Cherukuri, J. G. Duque, T. K. Leeuw, M. K. Lackey, C. H. Moran, V. C. Moore, J. L. Conyers, R. E. Smalley, H. K. Schmidt, *Carbon* **2007**, *45*, 2388.
[54] R. B. Weisman, *Anal. Bioanal. Chem.* **2010**, *396*, 1015.
[55] A. F. Gazdar, V. Kurvari, A. Virmani, L. Gollahon, M. Sakaguchi, M. Westerfield, D. Kodagoda, V. Stasny, H. T. Cunningham, I. I. Wistuba, *Int. J. Cancer* **1998**, *78*, 766.
[56] K. H. Allison, M. E. H. Hammond, M. Dowsett, S. E. McKernin, L. A. Carey, P. L. Fitzgibbons, D. F. Hayes, S. R. Lakhani, M. Chavez-MacGregor, J. Perlmutter, *J. Clin. Oncol.* **2020**, *38*, 1346.
[57] Z. Cohen, D. J. Alpert, A. C. Weisel, A. K. Ryan, A. Roach, S. Rahman, P. V. Gaikwad, S. B. Nicoll, R. M. Williams, *Adv. Opt. Mater.* **2024**, *12*, 2303324.